Substrate-Dependent Area-Selective Atomic Layer Deposition of Noble Metals from Metal beta-Diketonate Precursors

Zhang, Chao

American Chemical Society
2022-09-04

Zhang, C, Tois, E, Leskelae, M & Ritala, M 2022, 'Substrate-Dependent Area-Selective Atomic Layer Deposition of Noble Metals from Metal beta-Diketonate Precursors', Chemistry of Materials, vol. 34, pp. 8379-8388. https://doi.org/10.1021/acs.chemmater.2c02084

http://hdl.handle.net/10138/572703
10.1021/acs.chemmater.2c02084

CHEMISTRY OF MATERIALS

pubs.acs.org/cm

Article

Substrate-Dependent Area-Selective Atomic Layer Deposition of Noble Metals from Metal β-Diketonate Precursors

Chao Zhang,* Eva Tois, Markku Leskelä, and Mikko Ritala*

Cite This: *Chem. Mater.* 2022, 34, 8379−8388

Read Online

ACCESS | Metrics & More | Article Recommendations | Supporting Information

ABSTRACT: Area-selective ALD of Ir, Ru, and Rh with excellent substrate selectivity was achieved by using metal β-diketonates, i.e., $Ir(acac)_3$, $Ru(thd)_3$, and $Rh(acac)_3$, as precursors with either O_2 or air as a coreactant. Native SiO_2 and Ru were identified as growth surfaces while low-*k* SiOC, native oxide terminated Cu and Co, Al_2O_3, ZrO_2, and HfO_2 were identified as the nongrowth surfaces. UV (254 nm) irradiation in air was proven efficient to activate the low-*k* SiOC surface for the noble metal growth. UV exposure of 1 min was sufficient for the growth activation yet without causing any damage to the low-*k* material. Selective growth of the noble metals was successfully demonstrated on a UV-irradiated test chip that has micro- and nanometer-scale low-*k* SiOC/Cu patterns. At the optimal selective deposition temperatures, that is 225 °C for the Ir, 300 °C for the Ru, and 250 °C for the Rh, films with a thickness of at least 10 nm for Ir and ∼30 nm for Ru and Rh can be selectively deposited on the UV-activated low-*k* SiOC regions, while no growth occurs on Cu regions, as characterized by SEM, TEM, and EDS.

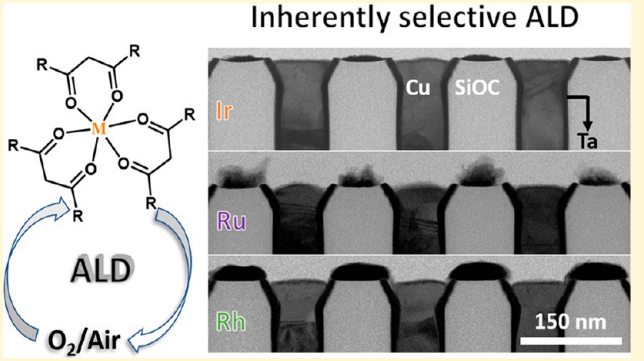

INTRODUCTION

Device downsizing along Moore's law[1] and the adoption of new 3D device architectures[2] bring challenges to the conventional lithographic patterning techniques. While extreme ultraviolet (EUV) lithography and multipatterning techniques enable future scaling, pattern misalignment, such as edge placement error (EPE), becomes a bottleneck in integrated circuit (IC) fabrication at advanced technology nodes, such as 5 nm and beyond.[3] To mitigate this technical challenge, self-aligned thin-film patterning was proposed and has received extensive research interest.[4−6]

Area-selective atomic layer deposition (AS-ALD) is a self-aligned thin film deposition process that exploits local chemical differences to direct thin film growth on desired substrate areas while no growth occurs on the others.[7] The chemical differences on a substrate surface either already exist, for example, on IC devices (semiconductors, insulators, metals) or are created by surface passivation or activation. Major parts of the earlier research focus on the surface passivation route wherein selected parts of the substrate are made inert toward the ALD chemistry. As a result, the ALD growth is prevented on the passivated substrate areas while the growth proceeds on the others, and a self-aligned growth of thin-film patterns is therefore achieved. Self-assembled monolayers (SAMs)[8−11] with $-CH_3$ tail groups are commonly used as the surface passivator to prevent the ALD growth. Inert polymers[12−14] have also been studied as passivation layers, though to a lesser extent compared to the SAMs. In contrast to surface passivation, AS-ALD by surface activation utilizes reaction activators to promote the ALD growth on an otherwise inert substrate, so that the film-forming reactions proceed only on the activator-seeded substrate areas and not on the others. Noble metals and their oxides such as Pt,[15,16] Ir,[15] and RuO_x[17] have been studied as the catalytic seed layers for AS-ALD of Pt, Fe_2O_3, NiO, and Ru. Our recent work showed that CuO_x can be used as a catalytic seed layer for area-selective molecular layer deposition of polyimide (AS-MLD) at deposition temperatures of 200−210 °C.[18]

While many successes have been achieved in AS-ALD by surface passivation and activation, in most cases the processes are not fully self-aligned in a sense that patterning of the passivation or activation layers before the ALD process is required. Photolithography was used by Chen et al.[11] to create hydrogen-terminated Si/SiO_2 patterns for selective grafting of an octadecyltrichlorosilane (ODTS) SAM onto the SiO_2 areas or a 1-alkene SAM onto the hydrogen-terminated Si areas. AS-ALD of Pt on SiO_2 and HfO_2 on the hydrogen-terminated Si was thereby achieved. Polymer films such as poly(methyl methacrylate) (PMMA) and polyvinylpyrrolidone (PVP) were

Received: July 11, 2022
Revised: August 26, 2022
Published: September 5, 2022

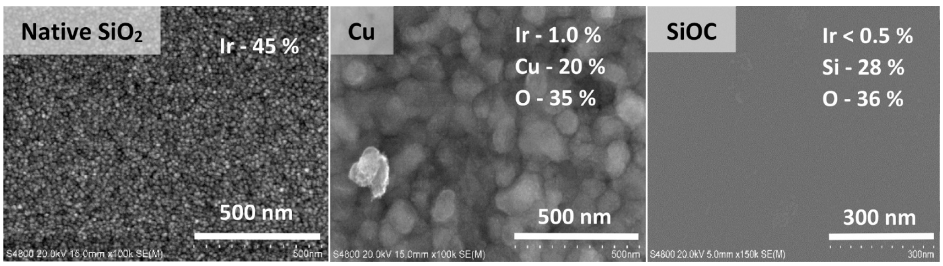

Figure 1. SEM images of the Ir growth at 250 °C for 1000 cycles on native SiO_2, native oxide covered Cu, and SiOC. Insets: XPS atomic percentages with the rest being adventitious carbon and oxygen.

photolithographically patterned by Färm et. al for AS-ALD of Al_2O_3, TiO_2, Ir, Ru, and Pt.[12,13] Electron beam induced deposition (EBID) was utilized to write Pt seed layer patterns on Al_2O_3 for AS-ALD of Pt.[19] The prepatterning of the growth inhibitors or activators not only raises misalignment issues but also complicates the whole patterning process. In recent research, SAMs[9,20−22] and small molecular inhibitors (SMIs)[23−25] that selectively adsorb onto specific materials on the surface and not on the others have been explored for fully self-aligned AS-ALD. Yu et al.[9] studied selective adsorption of dodecanethiol onto Cu and octadecylphosphonic acid onto native oxide-terminated Al, both with SiO_2 as the nonadsorption surface. AS-MLD of SiOC on SiO_2 versus Cu and native oxide-terminated Al was achieved. Mameli et al.[24] exploited selective adsorption of Hacac SMI for AS-ALD of SiO_2 on GeO_2, SiN, and SiO_2, where the SMI inhibitor does not adsorb, while the growth was prevented on surfaces where the Hacac inhibitor adsorbed, such as TiO_2, HfO_2, and Al_2O_3.

In addition to the above-mentioned strategies for the self-aligned AS-ALD, the concept of inherently selective ALD chemistry with inherent material selectivity has been brought up occasionally. Mackus noted that self-aligned AS-ALD can be achieved in making IC devices by developing ALD processes that have a significant nucleation difference between various materials, ideally, an immediate nucleation on certain materials versus an infinite nucleation delay on others. The nucleation differences result in selectivity during the initial ALD cycles, as long as no nucleation occurs on the nongrowth surface.[26] This substrate-dependent AS-ALD has an obvious advantage over the surface passivation or activation approaches in that there is no need for separate surface modification before the ALD process. Therefore, the use of surface modifiers and their patterning and removal processes are avoided. Despite its simplicity and efficiency, the application of the substrate-dependent AS-ALD is often limited by its poor selectivity, allowing selective deposition of a film only a few nanometers thick.[27−30] Corrective etching processes have therefore been developed to remove periodically the unwanted growth from the nongrowth areas which significantly extends the selectivity.[31−35]

Here, inherently area-selective ALD of Ir, Ru, and Rh from β-diketonate precursors is reported. The combustion-type noble metal ALD processes were found to be highly selective toward the underlying materials. Native SiO_2, low-k SiOC, and Cu were mostly studied as the growth surfaces. Other surfaces including Al_2O_3, ZrO_2, HfO_2, Co, and Ru were also examined. The selectivity was also verified on a test chip that has micro- and nanometer scale patterns of low-k SiOC/Cu. To realize selective growth of Ir, Ru, and Rh on low-k SiOC versus Cu, surface activation of the low-k SiOC by UV irradiation is needed. The similarities of the studied noble metal ALD processes, i.e., the use of metal β-diketonates as precursors and O_2-activated ligand combustion as the film growth reaction, might indicate many possibilities for inherent selectivity from similar ALD processes.

EXPERIMENTAL SECTION

The film deposition was carried out in a commercial hot-wall flow-type F120 ALD reactor (ASM Microchemistry Ltd., Finland). The reactor pressure was ∼10 mbar during the deposition. Nitrogen (Linde Gas, 99.999%) was used as the carrier and purge gases. Ir films were deposited from $Ir(acac)_3$ (acac = acetylacetonato) (99.9%, ABCR) and O_2 (99.9999%, Linde Gas),[36] Ru films were created from $Ru(thd)_3$ (thd = 2,2,6,6-tetramethyl-3,5-heptanedionato) (Volatec, Finland) and air,[37] and Rh films were created from $Rh(acac)_3$ (Volatec, Finland) and O_2.[38] Pulse and purge times of 1 s were used in all ALD processes. The 5 × 5 cm^2 sized Si pieces covered with different top layers, i.e., native SiO_2, SiOC, Cu, Co, Ru, Al_2O_3, ZrO_2, and HfO_2, were used as the substrates for the film growth. Al_2O_3 layers with thicknesses of ∼7.6 or 100 nm were prepared by ALD from $AlCl_3/H_2O$[39] or TMA/H_2O.[40] ZrO_2 and HfO_2 films with a thickness of ∼4.5 nm were prepared by ALD from tetrakisdimethylamino zirconium and hafnium with water as a coreactant.[41] A structure of 50 nm Co/100 nm SiO_2/Si had been prepared by depositing Co with physical vapor deposition (PVD). A structure of 5 nm Ru/80 nm SiO_2/Si had been prepared by depositing Ru with CVD. UV light with a primary wavelength of 254 nm was used to activate the SiOC surface. Unless otherwise noted, all surfaces were used as received without any chemical pretreatment, meaning that a native oxide was present on the Cu and Co surfaces.

The hydrophilicities of SiOC films with different UV irradiation times were evaluated by water contact angle measurements (CAM100, KSV Instruments, Finland). Thicknesses and refractive indices of the SiOC films were measured by an FS-1 multiwavelength ellipsometer (Film Sense, Lincoln, NE, U.S.A.). Bonding information of the SiOC films was obtained from attenuated total reflection Fourier transform infrared (ATR-FTIR) spectra (Thermo Fisher iS50, U.S.A.). Scanning electron microscopy (SEM) was utilized to observe the growth of the Ir, Ru, and Rh films on different surfaces. A combination of SEM, energy dispersive X-ray spectroscopy (EDS), and transmission electron microscopy (TEM) was used to confirm the selective deposition of Ir, Ru, and Rh on UV-activated SiOC regions versus the native oxide covered Cu regions on a test chip. A Hitachi S-4800 field emission scanning electron microscope (Hitachi, Tokyo, Japan) equipped with an INCA 350 EDS spectrometer was used for the SEM and EDS characterization. Bright field scanning transmission electron microscopy (STEM) was performed using a Hitachi High-Tech HD-2700B transmission electron microscope that was operated at 200 kV. X-ray photoelectron spectroscopy (XPS) measurements were conducted for elemental identification and quantification. A K-alpha X-ray photoelectron spectrometer system (Thermo Fisher) using Al Kα radiation at 1486.7 eV was operated with a pass energy of 200 eV for survey scans and 30 eV for high-resolution scans.

RESULTS AND DISCUSSION

Selectivity of the ALD Ir Process on Blanket Native SiO_2, Cu, and Low-k SiOC. Selective deposition of Ir from $Ir(acac)_3$ and O_2[36] was first tested on three blanket surfaces:

https://doi.org/10.1021/acs.chemmater.2c02084
Chem. Mater. 2022, 34, 8379−8388

native SiO_2, low-k SiOC, and native oxide covered Cu. SiOC is carbon-doped SiO_2, a low-k material commonly used as an interlayer dielectric (ILD) in ICs. Ir films were deposited at 250 °C with a cycle number of 1000. SEM and XPS were used to characterize the Ir growth on the different surfaces. As shown in the SEM images in Figure 1, a continuous and pinhole-free Ir film was deposited on the native SiO_2, whereas no visible growth was found on Cu and SiOC. XPS measurements further confirmed the substrate-dependent growth; the Ir signal was measured on the native SiO_2 with no Si signal being detected from the underlying substrate because of the growth of a thick Ir film, and the reported thickness of an Ir film grown on in situ prepared Al_2O_3 with 1000 cycles is ∼30 nm.[36] By contrast, only 1.0 at % Ir was measured on Cu, and no Ir signal was detected on SiOC within the XPS detection limit of ∼0.5 at % for Ir.

The lack of Ir growth on SiOC is attributed to the inertness of $-CH_3$ terminal groups toward the ALD precursors, which prevents the growth initiation on SiOC. Native SiO_2 and native oxide covered Cu are both terminated with −OH groups, which are well-known reactive sites for ALD precursors. Therefore, selective adsorption of precursors or coreactants as a well-studied mechanism for substrate-dependent selectivity[26] cannot explain the selective Ir growth on the native SiO_2 over the native oxide terminated Cu. A new selectivity mechanism is thus proposed, that is, surface passivation by byproducts, occurring during the initial nucleation stage. The study on the adsorption mechanism of $Ir(acac)_3$ on silica and alumina powder by Silvennoinen et al.[42] confirmed that a ligand exchange reaction took place between $Ir(acac)_3$ and the surface −OH groups. The released Hacac byproduct molecules appeared to selectively adsorb onto the alumina support over the silica support, resulting in the blocking of the Ir adsorption onto the alumina support. Surface blocking by the Hacac byproducts was reported also by Vuori et al.[43,44] In addition, the efficiency of Hacac as a small molecular inhibitor (SMI) to prevent ALD chemistry on Al_2O_3, TiO_2, and HfO_2 has been demonstrated in AS-ALD of SiO_2 on GeO_2, SiN_x, SiO_2, and WO_3.[24] The selectivity arises from the adsorption of Hacac on the Al_2O_3, TiO_2, and HfO_2 surfaces but not on the others. Yarbrough et al.[25] rationalized that the selective adsorption of SMIs relies on Lewis or Bronsted acid−base surface chemistry. Hacac exhibits primarily acidic characteristics and therefore preferentially bonds with more basic surfaces, such as Al_2O_3, ZrO_2, and HfO_2, rather than the acidic SiO_2. According to the literature,[25,45,46] copper oxides have comparable or even lower surface acidity values than the above-mentioned metal oxides, and native oxide covered Cu is therefore expected to bond strongly with Hacac. The adsorbed molecules passivate the substrate surfaces and thereby prevent the ALD growth, which is proposed to be a mechanism for the current observation of selective growth of Ir on native SiO_2 over Cu.

SiOC Surface Activation by UV Irradiation. One aim of this study is to realize Ir growth on low-k SiOC with Cu as the nongrowth surface. Because there is no growth on either of these surfaces as received, SiOC surface activation is needed for the Ir growth. So far, many approaches have been developed for low-k activation, including wet chemistry,[47] various plasma treatments,[48] and UV/O_3.[49] Wet chemistry is avoided here due to possible contamination from solvents. Plasma treatment could be efficient for the low-k activation, but the high-energy species in the plasma can seriously deteriorate material quality, causing an increased k value.[50] By contrast, UV irradiation in air is an efficient yet nondestructive approach for the low-k activation (Figure 2). Successful Ir growth on the low-k SiOC with 1 min of UV irradiation in air (Figure 3) proves the efficiency of UV

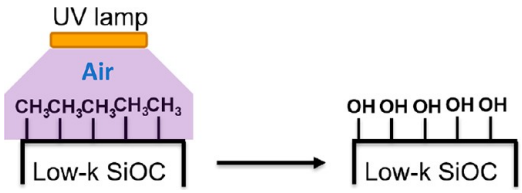

Figure 2. Schematic showing the surface activation mechanism.

irradiation on the low-k activation. The surface activation mechanism is suggested to be a conversion of surface methyl groups to hydroxyl groups with UV irradiation, as illustrated in Figure 2.

Although UV irradiation is recognized as a nondestructive method for the surface activation, a long-time UV irradiation might still cause detrimental impacts on low-k films. For example, an increase of the dielectric constant has been reported for the low-k SiOC, which is related to the breakage of Si−Me bonds that are replaced with Si−O bonds.[51] Also, a thickness decrease of the low-k thin film has been observed.[52] Therefore, it is important to study the effect of UV irradiation on the properties of the low-k SiOC to optimize the irradiation time for the growth activation.

The thickness and refractive index of the low-k SiOC films were monitored with ellipsometry after the UV irradiation. As shown in Table 1, the film thickness and refractive index remained the same for 30 min of UV irradiation. By contrast, IR spectra revealed an obvious change in the bonding structure of the low-k SiOC thin films (Figure 3a). After 1 min of UV exposure, the peak intensities from Si−Me remained the same as for the original sample. However, these peaks started to decrease obviously after 5 min of UV exposure, indicating a decreased density of methyl groups in the films. The loss of methyl groups from the low-k film is attributed to the breakage of Si-Me bonds induced by the UV irradiation.

Water contact angle (WCA) measurements were used to analyze the change of the surface hydrophilicity, which is closely related to the density of surface hydroxyl groups. As seen in Figure 3b, the WCA value measured on the low-k SiOC remained unchanged after 1 and 5 min of UV irradiation, suggesting no extensive formation of −OH groups on the low-k SiOC surface. After 10 min of UV irradiation, a large decrease of the WCA value was measured, from the original ∼90° to ∼70°. Thereafter, the WCA value decreased substantially with increasing UV exposure time. After 30 min of UV irradiation, the low-k SiOC surface became completely wetted with a WCA value close to zero. Although the surface hydrophilicity remained unchanged at 90°, a short UV exposure time of 1 min was enough to activate the Ir growth on the low-k SiOC, as evidenced by the SEM image (Figure 3b, inset), showing a continuous and pinhole-free layer of Ir grown on the low-k SiOC.

Selectivity Demonstration on a SiOC/Cu Test Chip. A test chip comprising low-k SiOC and Cu patterns (Figure 4a) was studied for the selective Ir growth. The chip was irradiated with UV light for 1 min and then taken to the ALD Ir process at 250 °C for 1000 cycles. As characterized by SEM (Figure 4b), selective deposition of Ir on the low-k SiOC with respect to Cu was achieved. Slight nucleation, however, was observed on Cu. Also, in some places, voids had developed in the Cu areas which

https://doi.org/10.1021/acs.chemmater.2c02084
Chem. Mater. 2022, 34, 8379−8388

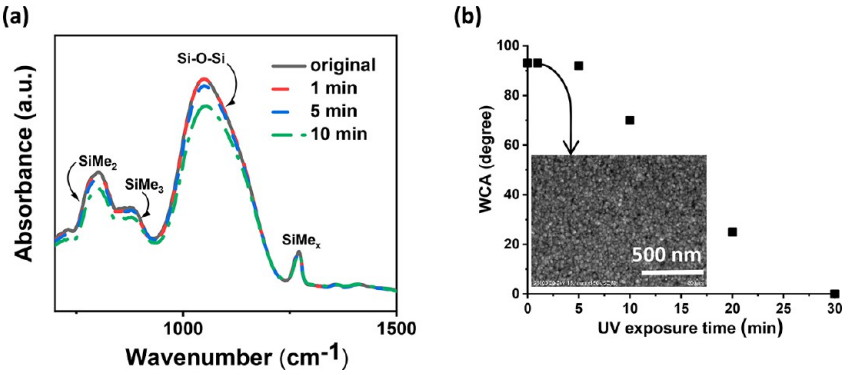

Figure 3. (a) FTIR absorption spectra and (b) WCAs of SiOC films with UV irradiation for various times. Inset: SEM image of Ir growth at 250 °C for 1000 cycles on SiOC with 1 min of UV irradiation.

Table 1. Ellipsometer Results for SiOC Films with Different UV Irradiation Times

UV irradiation time (min)	thickness (nm)	refractive index (633 nm)
0	86	1.49
1	86	1.49
30	87	1.49

could be due to etching caused by some kinds of acidic byproducts other than Hacac, which has previously been proven nonreactive for Cu etching.[53] Oxidation of Cu by O_2 is assumed to play a vital role in Cu etching. Therefore, lowering the deposition temperature to reduce extensive Cu oxidation should suppress the Cu etching reaction.

Optimization of the deposition conditions for better selectivity was attempted. The deposition temperature was expected to play a vital role in reducing the Cu etching and unwanted Ir nucleation on Cu areas. The ALD temperature window of the $Ir(acac)_3/O_2$ process was reported to be 225–375 °C.[36] The lower temperature limit of 225 °C is determined by the oxidative decomposition of the acac ligands of $Ir(acac)_3$, which drives the film growth. The upper limit of 375 °C is dictated by the thermal self-decomposition of $Ir(acac)_3$, which starts at 400 °C and eventually destroys the self-limiting growth mechanism. In our experiment, a lower deposition temperature of 200 °C was attempted since pure oxygen was used instead of air that was reported in the literature. Not a surprise, only a slight Ir nucleation was observed on SiOC at this temperature.

The deposition temperature was then increased to 225 °C, the reported lowest growth-enabling temperature. After 1000 cycles, SEM characterization confirmed the successful selective deposition of Ir films on the UV-activated low-*k* SiOC regions, and no Ir growth was found on Cu regions (Figure 5a). Also, at this temperature, the Cu etching was significantly reduced. Excellent selective growth of Ir films on the low-*k* SiOC versus Cu was achieved at 225 °C, which was also confirmed by TEM characterization (Figure 5b). Figure 5c shows energy dispersive X-ray maps of the Si, O, Cu, and Ir distributions on this sample. The strong Ir signal on the Si and O region indicates that Ir films were selectively deposited on SiOC, which is consistent with the observations from the SEM and TEM images. It is worth noting that we observed slightly less deposition of Ir in between the Cu trenches as compared to the Ir growth on areas away from the trenches. We assume that minor Cu migration might have happened there, which slows down the Ir growth in between the Cu trenches.

Ir Growth on Other Surfaces. The ALD Ir process was also studied on other materials, including Al_2O_3, ZrO_2, HfO_2, Co, and Ru. The Ir deposition was conducted at 250 °C for 1000

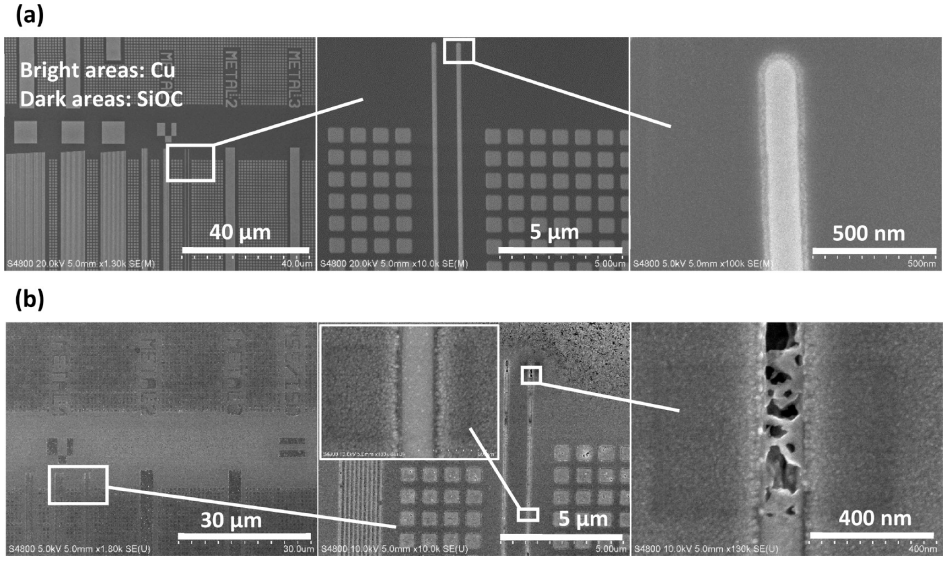

Figure 4. SEM images of (a) the UV-irradiated test chip and (b) the sample after the ALD Ir at 250 °C for 1000 cycles.

https://doi.org/10.1021/acs.chemmater.2c02084
Chem. Mater. 2022, 34, 8379−8388

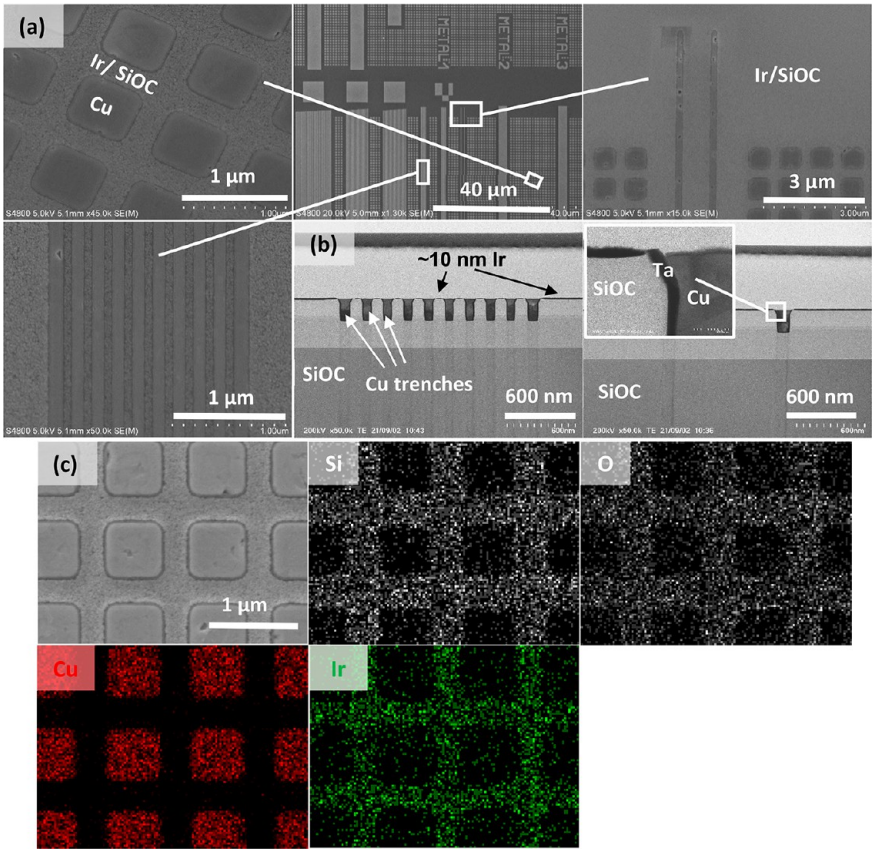

Figure 5. (a) SEM and (b) TEM images showing the selective growth of Ir on the UV irradiated test chip at 225 °C for 1000 cycles. (c) EDS maps show the distributions of Si, O, Cu, and Ir elements.

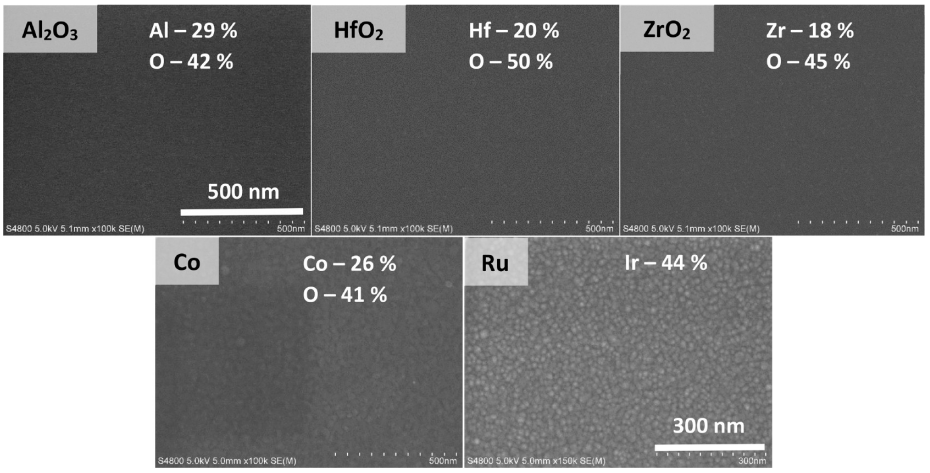

Figure 6. SEM images after the Ir growth on Al_2O_3, ZrO_2, HfO_2, Co, and Ru at 250 °C for 1000 cycles. Insets: XPS atomic percentages.

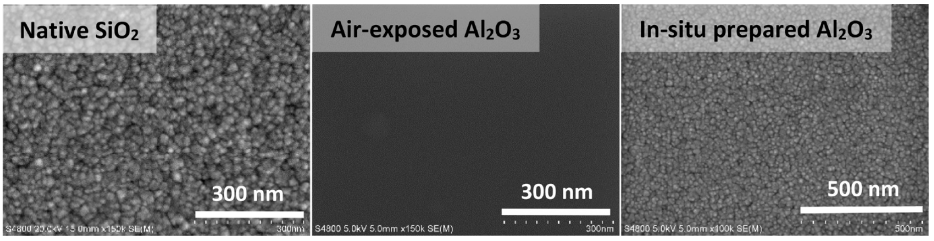

Figure 7. SEM images showing the Ir growth on reference Si, air-exposed Al_2O_3, and in situ prepared Al_2O_3; the Al_2O_3 thin films were grown from $AlCl_3$ and H_2O.

https://doi.org/10.1021/acs.chemmater.2c02084
Chem. Mater. 2022, 34, 8379−8388

cycles. As seen in SEM images (Figure 6), no Ir growth was observed on Al_2O_3, ZrO_2, and HfO_2. The lack of growth was further confirmed by XPS measurements with no Ir signal being detected on these surfaces. XPS measurements confirmed no Ir growth also on Co. By contrast, obvious Ir growth was identified on Ru with 44 at. % Ir being detected by XPS. While the lack of growth on metal (Cu, Co) and metal oxides (Al_2O_3, ZrO_2, HfO_2) is explained by the surface passivation by the read-sorption of the byproduct Hacac during the growth initiation stage, the Ir growth on Ru is attributed to the Ru catalyzed dissociation of molecular oxygen to reactive atomic oxygen, which combusts away adsorbed Hacac molecules, if any.[37] Therefore, the Ir growth proceeded on the Ru surface.

It is noteworthy that, in the original work on the $Ir(acac)_3/O_2$ process,[36] Ir thin films could be deposited on 5 nm thick Al_2O_3 films on Si. This Al_2O_3 layer was deposited by ALD from $AlCl_3$ and water right before the Ir deposition, which is different from our cases where the Al_2O_3-coated Si was exposed to ambient air before the Ir deposition. Also, in our experiment, the Ir growth was confirmed to take place on the in situ prepared Al_2O_3 but not on the air-exposed Al_2O_3, as shown in Figure 7. To better understand possible reasons causing the different Ir growth on the different seed layers, it is important to study how the history (precursors, air-exposure or not) of the Al_2O_3 seed layers affects the deposition.

Poor nucleation is a well-known issue in ALD of noble metals. Seed layers of metal oxides, typically Al_2O_3, or nucleation promoters such as $AlMe_3$, $AlMe_2Cl$, $ZnEt_2$, $AlCl_3$, etc., have been used to enhance the nucleation.[54] The nucleation enhancement is attributed to the maximization of reactive sites on the substrate surfaces. The Al_2O_3 seed layers in the ALD of Ir are suggested to increase the density of surface −OH groups, which serve as nucleation sites for the Ir growth. Thus, blocking of the surface −OH groups by atmospheric hydrocarbons could be a mechanism to explain the nongrowth of Ir on the air-exposed Al_2O_3. UV irradiation is supposed to remove hydrocarbon contaminations on the air-exposed Al_2O_3, thus, re-exposing surface −OH groups for the Ir deposition. However, we did not observe any Ir growth on the UV-irradiated Al_2O_3 surface, which does not support the surface blocking mechanism by the adventitious hydrocarbons.

Our second mechanistic hypothesis highlights the importance of surface Al−Cl groups for the Ir growth on an Al_2O_3 seed layer. ALD of Ir was tested on a series of in situ prepared Al_2O_3 layers grown from $AlCl_3$ and H_2O with different pulse sequences (Table 2). In addition, an in situ Al_2O_3 seed layer was deposited from TMA and H_2O for comparison.

The difference between experiment 1 and experiment 2 is in the ending of the ALD sequences for depositing the Al_2O_3 seed layers; in experiment 1 the ALD Al_2O_3 process was ended with the $AlCl_3$ pulse, while in experiment 2 it was ended with the H_2O pulse. In experiment 2, a significant delay in the Ir growth should be expected due to the low concentration of Al−Cl terminal groups on the Al_2O_3 seed layers. However, the Ir growth was successful with a continuous and pinhole-free layer being deposited, as shown in the SEM image (Figure 8). Also, mirror-like Ir film was seen by the naked eye. The successful Ir growth might be explained by the fact that one H_2O pulse does not consume all the Al−Cl terminal groups, and already residual amounts are sufficient for a successful Ir growth. Indeed, insertion of an additional five H_2O pulses between the ALD Al_2O_3 and the ALD Ir processes significantly decreased the Ir growth (experiment 3). The resulting Ir film was barely seen by the naked eye and consisted of separate islands as viewed with SEM (Figure 8).

Furthermore, an Al_2O_3 thin film deposited from TMA and H_2O was tested as a seed layer for the Ir growth (experiment 5). The Ir growth was problematic as only slight growth was observed by naked eye, and growth of Ir islands was observed with SEM (Figure 8). To conclude, Al−Cl terminal groups are most likely essential for the Ir growth once an Al_2O_3 seed layer is used for the growth. On the other hand, complete blocking of the Ir growth on Al_2O_3, no matter whether deposited from $AlCl_3$ or TMA, also needs air exposure.

ALD of Ru from $Ru(thd)_3$. Deposition of Ru thin films was attempted from $Ru(thd)_3$ and an oxygen-containing coreactant following the procedure in ref 37. Three coreactants were tested, O_2, air, and an O_2−H_2O combination. Regardless of the deposition conditions, no success was achieved using O_2 as the coreactant; either no film or only scattered film islands were grown on Si and in situ grown Al_2O_3. Ru growth from $Ru(thd)_3$ was successful, however, when air was used as the coreactant. The SEM image (Figure 9) presents the successful Ru growth on Al_2O_3 grown in situ from $AlCl_3$ and H_2O. Ru growth on a native oxide-terminated Si wafer was also successful.

Deposition of Ru from $Ru(thd)_3$ and the O_2−H_2O combination at 300 °C was conducted to verify that the success of the Ru growth using air instead of oxygen can be attributed to the presence of H_2O in the air. As shown in Figure 10, the use of the O_2−H_2O combination as a coreactant to $Ru(thd)_3$ made the Ru growth successful. Ru growth from $Ru(thd)_3$ failed when either O_2 or H_2O alone (Figure 10) was used as the coreactant.

Selectivity of the ALD of Ru from $Ru(thd)_3$ and air was studied on native oxide-terminated Si, low-*k* SiOC, and native oxide-terminated Cu at 300 and 350 °C for 1000 cycles. At 300 °C, substantial growth was observed on Si, while no Ru growth occurred on SiOC and Cu (Figure S1). Therefore, an excellent selectivity was achieved between Si versus low-*k* SiOC and Cu. Similar to the ALD Ir process, no Ru growth was found on Al_2O_3, ZrO_2, and HfO_2 at 300 °C for 1000 cycles, as characterized by SEM (Figure S1). At 350 °C, selective growth of Ru on Si was also demonstrated. No visible growth was observed on Cu, but some Ru growth was visible on the leading edge of the low-*k* SiOC sample. At 350 °C the unexpected growth on SiOC is assumed to be caused by oxidation of the terminal CH_3 groups to OH groups by the air pulses. The lack of growth is believed to be caused by a similar mechanism as in the ALD Ir process. Hacac and Hthd are both diketones. Their chemical structures are similar to each other, with the only difference in the substituent groups, as shown in Figure 11. The interaction of Hthd with the substrate surfaces is therefore expected to be similar to that of Hacac, which bonds favorably with more basic surfaces. The selectivity mechanism in the $Ru(thd)_3$/air process is thus proposed to be similar to that of the $Ir(acac)_3/O_2$ process, that is, selective adsorption of the

Table 2. Ir Growth on Al_2O_3-Seeded Si at 250 °C

ALD code	ALD sequence	resulting film
1	50 (H_2O−$AlCl_3$) + 1000 ($Ir(acac)_3$−O_2)	mirror-like film
2	50 ($AlCl_3$−H_2O) + 1000 ($Ir(acac)_3$−O_2)	mirror-like film
3	50 ($AlCl_3$−H_2O) + 5 (H_2O) + 1000 ($Ir(acac)_3$−O_2)	very thin film
4	1000 (H_2O−$AlCl_3$) + 1000 ($Ir(acac)_3$−O_2)	mirror-like film
5	1000 (H_2O−TMA) + 1000 ($Ir(acac)_3$−O_2)	very thin film

https://doi.org/10.1021/acs.chemmater.2c02084
Chem. Mater. 2022, 34, 8379−8388

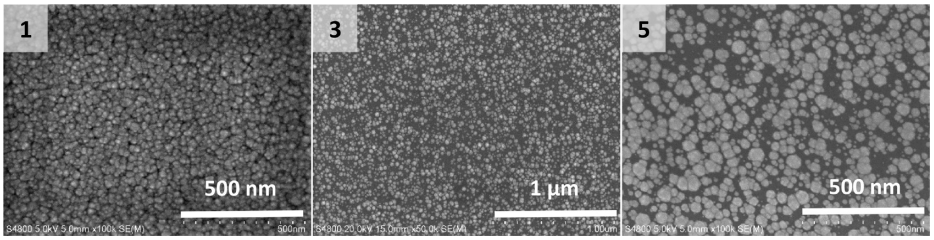

Figure 8. SEM images of the Ir films grown at 250 °C for 1000 cycles on the different in situ prepared Al_2O_3 samples with the numbers referring to Table 2.

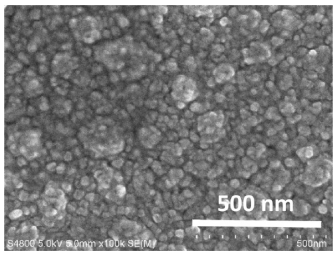

Figure 9. SEM image of a Ru film grown from $Ru(thd)_3$ and air at 350 °C on in situ prepared Al_2O_3.

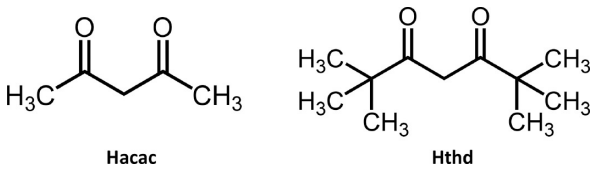

Figure 11. Chemical structures of Hacac and Hthd.

byproduct Hthd on more basic surfaces such as the native oxide covered copper, Al_2O_3, HfO_2, and ZrO_2 while not on the acidic SiO_2. The adsorbed Hthd efficiently passivates these surfaces and prevents the Ru ALD growth.

ALD of Ru was attempted also at a temperature below 300 °C. However, no Ru growth occurred on any surface already at 250 °C. Thus, selective deposition of Ru on UV-activated SiOC versus Cu was demonstrated on the test chip at 300 °C for 1000 cycles. Although some Cu etching was observed after the deposition, excellent selective growth of Ru on the UV-activated SiOC regions over the Cu regions was achieved, as characterized by SEM (Figure 12a), TEM (Figure 12b), and EDS mapping (Figure 12c).

ALD of Rh from $Rh(acac)_3/O_2$. A selectivity similar to those of the Ir and Ru processes was also observed in the $Rh(acac)_3/O_2$ process[38] at 250 °C. Native SiO_2 and UV-activated SiOC were identified as the growth surfaces, while native oxide covered Cu, SiOC, Al_2O_3, ZrO_2, and HfO_2 were identified as the nongrowth surfaces. Excellent selectivity was demonstrated with an Rh growth for 1000 cycles at 250 °C. On the test chip, Rh thin films with a thickness of ∼30 nm were selectively deposited on the UV-activated SiOC regions, while no growth was measured on the Cu regions, as characterized by SEM (Figure 13a), TEM (Figure 13b), and EDS mapping (Figure 13c). The similar selective growth behavior observed in the three noble metal ALD processes makes us believe that the substrate selectivity is inherent to the ALD processes that use β-diketonates as metal precursors and O_2-based ligand combustion as the film-forming reaction.

CONCLUSIONS

ALD of noble metals of Ir, Ru, and Rh from metal β-diketonate precursors with either oxygen or air as the coreactant was proven to exhibit excellent inherent surface selectivity. Native SiO_2, UV-activated SiOC, and Ru were identified as growth surfaces, while native oxide terminated Cu and Co, Al_2O_3, ZrO_2, and HfO_2 were identified as the nongrowth surfaces. The selectivity mechanism is assumed to be the surface passivation by the byproduct readsorption, occurring during the growth initiation stage. The byproducts Hacac or Hthd, released from the ligand exchange reaction between the metal β-diketonate precursors ($Ir(acac)_3$, $Ru(thd)_3$, and $Rh(acac)_3$) and surface OH groups present on substrate surfaces selectively adsorb and passivate more alkaline CuO_x, CoO_x, Al_2O_3, ZrO_2, and HfO_2 surfaces versus native SiO_2 and UV-activated SiOC surfaces. The growth on Ru is attributed to the catalytic dissociation of O_2 to more reactive atomic oxygen, which combusts the readsorbed Hacac, if any, to CO_2 and H_2O.

The inherent substrate selectivity was successfully demonstrated on a test chip with micro- and nanometer scale Cu/SiOC patterns. UV exposure for 1 min in air was proven efficient to activate the noble metal growth on the SiOC surface without causing any damage to the low-k SiOC. Excellent selective growth of Ir, Ru, and Rh on the UV-activated SiOC regions versus Cu regions was achieved. For example, an Ir film at least 10 nm thick can be selectively deposited on the low-k SiOC regions, while no growth occurs on the Cu regions, as

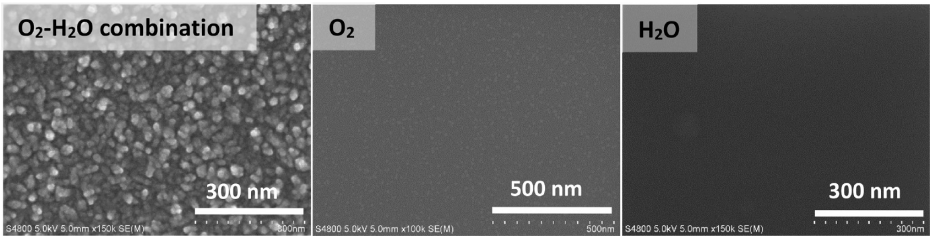

Figure 10. SEM images of the Ru growth on Si at 300 °C from $Ru(thd)_3$ and the O_2−H_2O combination (left), O_2 alone (middle), or H_2O alone (right).

https://doi.org/10.1021/acs.chemmater.2c02084
Chem. Mater. 2022, 34, 8379−8388

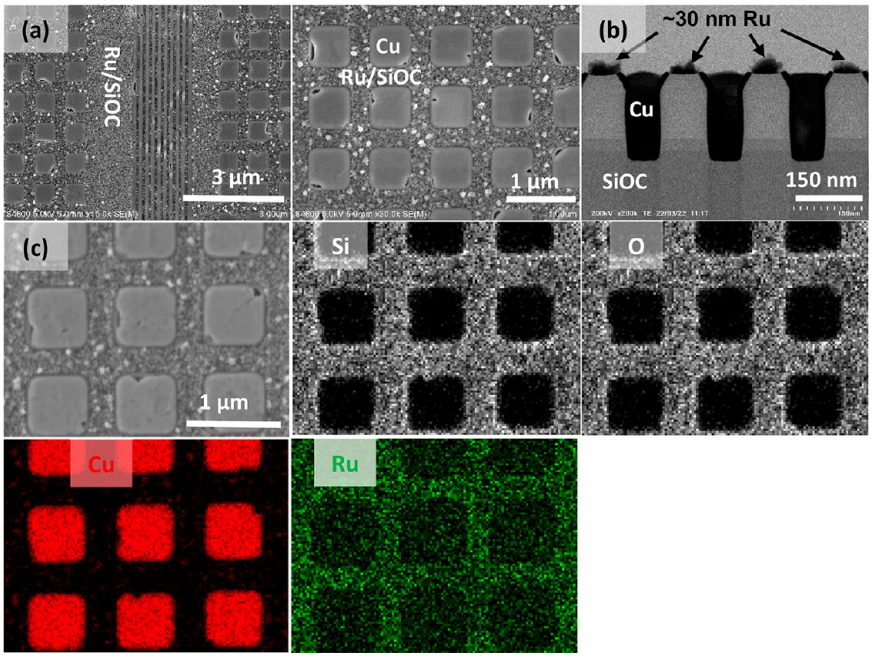

Figure 12. (a) SEM and (b) TEM images showing the selective growth of Ru on the UV irradiated test chip at 300 °C for 1000 cycles. (c) EDS maps showing the distributions of Si, O, Cu, and Ru elements.

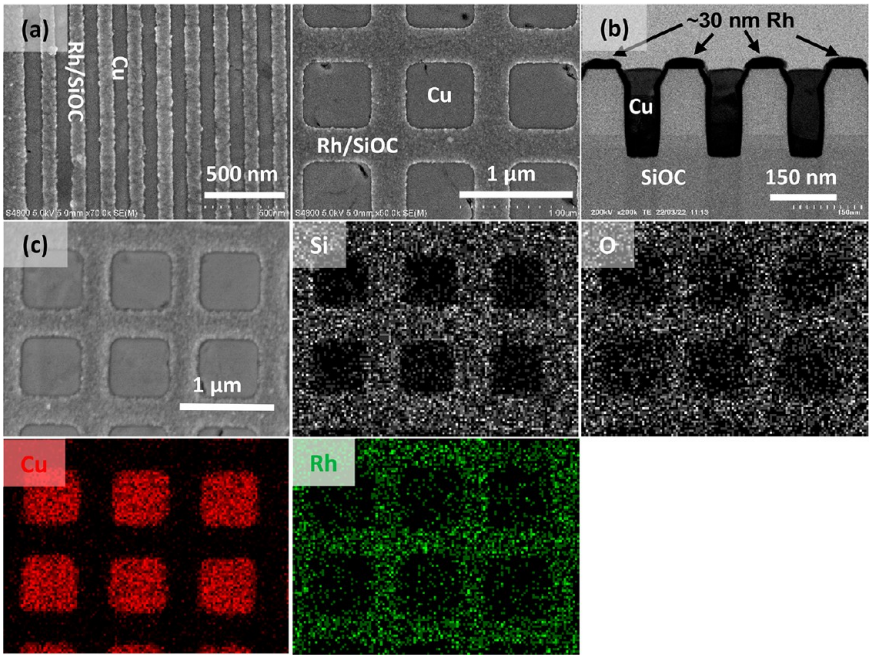

Figure 13. (a) SEM and (b) TEM images showing the selective growth of Rh on the UV irradiated test chip at 250 °C for 1000 cycles. (c) EDS maps showing the distributions of Si, O, Cu, and Rh elements.

characterized by SEM, TEM, and EDS. The similarities of the noble metal ALD processes, i.e., the use of metal β-diketonates as precursors and oxygen-activated ligand combustion as the film-forming reaction, indicate further possibilities for excellent substrate selectivity in many ALD processes alike.

■ ASSOCIATED CONTENT

Supporting Information

The Supporting Information is available free of charge at https://pubs.acs.org/doi/10.1021/acs.chemmater.2c02084.

SEM images after the Ru growth on native SiO_2, Cu, Al_2O_3, ZrO_2, and HfO_2 at 300 °C for 1000 cycles (PDF)

■ AUTHOR INFORMATION

Corresponding Authors

Chao Zhang − *Department of Chemistry, University of Helsinki, Helsinki, Uusimaa 00014, Finland;* orcid.org/0000-0002-9273-2289; Email: chao.zhang@helsinki.fi

Mikko Ritala − *Department of Chemistry, University of Helsinki, Helsinki, Uusimaa 00014, Finland;* orcid.org/0000-0002-6210-2980; Email: mikko.ritala@helsinki.fi

https://doi.org/10.1021/acs.chemmater.2c02084
Chem. Mater. 2022, 34, 8379−8388

Authors

Eva Tois − *ASM Microchemistry Oy, Helsinki, Uusimaa 00560, Finland*

Markku Leskelä − *Department of Chemistry, University of Helsinki, Helsinki, Uusimaa 00014, Finland;* orcid.org/0000-0001-5830-2800

Complete contact information is available at: https://pubs.acs.org/10.1021/acs.chemmater.2c02084

Notes

The authors declare no competing financial interest.

■ ACKNOWLEDGMENTS

Financial support from ASM Microchemistry, the Academy of Finland (ALD of Noble Metals and Their Compounds, Decision Number 309552), and the China Scholarship Council (File No. 201507040043) are gratefully acknowledged. The authors thank Marianna Kemell and Marko Vehkamäki for the thoughtful discussion on SEM measurements. The work was done in the ALD Centre Finland research infrastructure.

■ REFERENCES

(1) Moore, G. E. Cramming More Components onto Integrated Circuits. *Electronics* **1965**, *38* (8), 33−35.

(2) International Roadmap for Devices and Systems (IRDS). *2016 Edition White Papers*. https://irds.ieee.org/editions/2016 (accessed 2021-12-11).

(3) Mohanty, N.; Smith, J. T.; Huli, L.; Pereira, C.; Raley, A.; Kal, S.; Fonseca, C.; Sun, X.; Burns, R. L.; Farrell, R. A. EPE Improvement Thru Self-Alignment via Multi-Color Material Integration. *SPIE Advanced Lithography* **2017**, *10147*, 1014704.

(4) Clark, R.; Tapily, K.; Yu, K.-H.; Hakamata, T.; Consiglio, S.; O'Meara, D.; Wajda, C.; Smith, J.; Leusink, G. Perspective: New Process Technologies Required for Future Devices and Scaling. *APL Mater.* **2018**, *6* (5), 058203.

(5) Zhang, C.; Leskelä, M.; Ritala, M. Self-Aligned Thin-Film Patterning by Area-Selective Etching of Polymers. *Coatings* **2021**, *11* (9), 1124.

(6) Parsons, G. N.; Clark, R. D. Area-selective deposition: Fundamentals, applications, and future outlook. *Chem. Mater.* **2020**, *32* (12), 4920−4953.

(7) Mackus, A. J. M.; Bol, A. A.; Kessels, W. M. The Use of Atomic Layer Deposition in Advanced Nanopatterning. *Nanoscale* **2014**, *6* (19), 10941−10960.

(8) Färm, E.; Kemell, M.; Ritala, M.; Leskelä, M. Selective-Area Atomic Layer Deposition with Microcontact Printed Self-Assembled Octadecyltrichlorosilane Monolayers as Mask Layers. *Thin Solid Films* **2008**, *517* (2), 972−975.

(9) Yu, X.; Bobb-Semple, D.; Oh, I.-K.; Liu, T.-L.; Closser, R. G.; Trevillyan, W.; Bent, S. F. Area-Selective Molecular Layer Deposition of a Silicon Oxycarbide Low-k Dielectric. *Chem. Mater.* **2021**, *33* (3), 902−909.

(10) Chen, R.; Kim, H.; McIntyre, P. C.; Bent, S. F. Investigation of Self-Assembled Monolayer Resists for Hafnium Dioxide Atomic Layer Deposition. *Chem. Mater.* **2005**, *17* (3), 536−544.

(11) Chen, R.; Bent, S. F. Chemistry for Positive Pattern Transfer Using Area-Selective Atomic Layer Deposition. *Adv. Mater.* **2006**, *18* (8), 1086−1090.

(12) Färm, E.; Kemell, M.; Santala, E.; Ritala, M.; Leskelä, M. Selective-Area Atomic Layer Deposition Using Poly(vinyl pyrrolidone) as a Passivation Layer. *J. Electrochem. Soc.* **2010**, *157* (1), K10−K14.

(13) Färm, E.; Kemell, M.; Ritala, M.; Leskelä, M. Selective-Area Atomic Layer Deposition Using Poly(methyl methacrylate) Films as Mask. *J. Phys. Chem. C* **2008**, *112* (40), 15791−15795.

(14) Sinha, A.; Hess, D. W.; Henderson, C. L. Area-Selective ALD of Titanium Dioxide Using Lithographically Defined Poly(methyl methacrylate) Films. *J. Electrochem. Soc.* **2006**, *153* (5), G465−G469.

(15) Singh, J. A.; Thissen, N. F. W.; Kim, W.-H.; Johnson, H.; Kessels, W. M.; Bol, A. A.; Bent, S. F.; Mackus, A. J. M. Area-Selective Atomic Layer Deposition of Metal Oxides on Noble Metals through Catalytic Oxygen Activation. *Chem. Mater.* **2018**, *30* (3), 663−670.

(16) Mackus, A. J. M.; Thissen, N.; Mulders, J.; Trompenaars, P.; Verheijen, M.; Bol, A. A.; Kessels, W. M. Direct-Write Atomic Layer Deposition of High-Quality Pt Nanostructures: Selective Growth Conditions and Seed Layer Requirements. *J. Phys. Chem. C* **2013**, *117* (20), 10788−10798.

(17) Färm, E.; Lindroos, S.; Ritala, M.; Leskelä, M. Microcontact Printed RuO_x Film as an Activation Layer for Selective-Area Atomic Layer Deposition of Ruthenium. *Chem. Mater.* **2012**, *24* (2), 275−278.

(18) Zhang, C.; Vehkamäki, M.; Pietikäinen, M.; Leskelä, M.; Ritala, M. Area-Selective Molecular Layer Deposition of Polyimide on Cu through Cu-Catalyzed Formation of a Crystalline Interchain Polyimide. *Chem. Mater.* **2020**, *32* (12), 5073−5083.

(19) Mackus, A. J. M.; Dielissen, S.; Mulders, J.; Kessels, W. M. Nanopatterning by Direct-Write Atomic Layer Deposition. *Nanoscale* **2012**, *4* (15), 4477−4480.

(20) Liu, T.-L.; Bent, S. F. Area-Selective Atomic Layer Deposition on Chemically Similar Materials: Achieving Selectivity on Oxide/Oxide Patterns. *Chem. Mater.* **2021**, *33* (2), 513−523.

(21) Liu, T.-L.; Nardi, K. L.; Draeger, N.; Hausmann, D. M.; Bent, S. F. Effect of Multilayer versus Monolayer Dodecanethiol on Selectivity and Pattern Integrity in Area-Selective Atomic Layer Deposition. *ACS Appl. Mater. Interfaces* **2020**, *12* (37), 42226−42235.

(22) Bobb-Semple, D.; Nardi, K. L.; Draeger, N.; Hausmann, D. M.; Bent, S. F. Area-Selective Atomic Layer Deposition Assisted by Self-Assembled Monolayers: A Comparison of Cu, Co, W, and Ru. *Chem. Mater.* **2019**, *31* (5), 1635−1645.

(23) Merkx, M. J. M.; Vlaanderen, S.; Faraz, T.; Verheijen, M. A.; Kessels, W. M.; Mackus, A. J. M. Area-Selective Atomic Layer Deposition of TiN Using Aromatic Inhibitor Molecules for Metal/Dielectric Selectivity. *Chem. Mater.* **2020**, *32* (18), 7788−7795.

(24) Mameli, A.; Merkx, M. J. M.; Karasulu, B.; Roozeboom, F.; Kessels, W. M.; Mackus, A. J. M. Area-Selective Atomic Layer Deposition of SiO_2 Using Acetylacetone as a Chemoselective Inhibitor in an ABC-Type Cycle. *ACS Nano* **2017**, *11* (9), 9303−9311.

(25) Yarbrough, J.; Shearer, A. B.; Bent, S. F. Next Generation Nanopatterning Using Small Molecule Inhibitors for Area-Selective Atomic Layer Deposition. *J. Vac. Sci. Technol. A* **2021**, *39* (2), 021002.

(26) Mackus, A. J. M.; Merkx, M. J. M.; Kessels, W. M. From the Bottom-Up: Toward Area-Selective Atomic Layer Deposition with High Selectivity. *Chem. Mater.* **2019**, *31* (1), 2−12.

(27) McDonnell, S.; Longo, R. C.; Seitz, O.; Ballard, J. B.; Mordi, G.; Dick, D.; Owen, J. H. G.; Randall, J. N.; Kim, J.; Chabal, Y. J.; Cho, K.; Wallace, R. M. Controlling the Atomic Layer Deposition of Titanium Dioxide on Silicon: Dependence on Surface Termination. *J. Phys. Chem. C* **2013**, *117* (39), 20250−20259.

(28) Atanasov, S. E.; Kalanyan, B.; Parsons, G. N. Inherent Substrate-Dependent Growth Initiation and Selective-Area Atomic Layer Deposition of TiO_2 Using "water-free" Metal-Halide/Metal Alkoxide Reactants. *J. Vac. Sci. Technol. A* **2016**, *34* (1), 01A148.

(29) Dick, D.; Ballard, J. B.; Longo, R. C.; Randall, J. N.; Cho, K.; Chabal, Y. J. Toward Selective Ultra-High-Vacuum Atomic Layer Deposition of Metal Oxides on Si(100). *J. Phys. Chem. C* **2016**, *120* (42), 24213−24223.

(30) Tao, Q.; Jursich, G.; Takoudis, C. Selective Atomic Layer Deposition of HfO_2 on Copper Patterned Silicon Substrates. *Appl. Phys. Lett.* **2010**, *96* (19), 192105.

(31) Vos, M. F. J.; Chopra, S. N.; Verheijen, M. A.; Ekerdt, J. G.; Agarwal, S.; Kessels, W. M.; Mackus, A. J. M. Area-Selective Deposition of Ruthenium by Combining Atomic Layer Deposition and Selective Etching. *Chem. Mater.* **2019**, *31* (11), 3878−3882.

(32) Song, S. K.; Kim, J.-S.; Margavio, H. R. M.; Parsons, G. N. Multimaterial Self-Aligned Nanopatterning by Simultaneous Adjacent

Thin Film Deposition and Etching. *ACS Nano* **2021**, *15* (7), 12276−12285.
(33) Saare, H.; Song, S. K.; Kim, J.-S.; Parsons, G. N. Effect of Reactant Dosing on Selectivity During Area-Selective Deposition of TiO_2 via Integrated Atomic Layer Deposition and Atomic Layer Etching. *J. Appl. Phys.* **2020**, *128* (10), 105302.
(34) Song, S. K.; Saare, H.; Parsons, G. N. Integrated Isothermal Atomic Layer Deposition/Atomic Layer Etching Supercycles for Area-Selective Deposition of TiO_2. *Chem. Mater.* **2019**, *31* (13), 4793−4804.
(35) Vallat, R.; Gassilloud, R.; Eychenne, B.; Vallée, C. Selective Deposition of Ta_2O_5 by Adding Plasma Etching Super-Cycles in Plasma Enhanced Atomic Layer Deposition Steps. *J. Vac. Sci. Technol. A* **2017**, *35* (1), 01B104.
(36) Aaltonen, T.; Ritala, M.; Sammelselg, V.; Leskelä, M. Atomic Layer Deposition of Iridium Thin Films. *J. Electrochem. Soc.* **2004**, *151* (8), G489−G492.
(37) Aaltonen, T.; Ritala, M.; Arstila, K.; Keinonen, J.; Leskelä, M. Atomic Layer Deposition of Ruthenium Thin Films from $Ru(thd)_3$ and Oxygen. *Chem. Vapor. Depos.* **2004**, *10* (4), 215−219.
(38) Aaltonen, T.; Ritala, M.; Leskelä, M. ALD of Rhodium Thin Films from $Rh(acac)_3$ and Oxygen. *Electrochem. Solid. St.* **2005**, *8* (8), C99−C101.
(39) Hiltunen, L.; Kattelus, H.; Leskelä, M.; Mäkelä, M.; Niinistö, L.; Nykänen, E.; Soininen, P.; Tiittad, M. Growth and Characterization of Aluminium Oxide Thin Films Deposited from Various Source Materials by Atomic Layer Epitaxy and Chemical Vapor Deposition Processes. *Mater. Chem. Phys.* **1991**, *28* (4), 379−388.
(40) Higashi, G. S.; Fleming, C. G. Sequential Surface Chemical Reaction Limited Growth of High Quality Al_2O_3 Dielectrics. *Appl. Phys. Lett.* **1989**, *55* (19), 1963−1965.
(41) Hausmann, D. M.; Kim, E.; Becker, J.; Gordon, R. G. Atomic Layer Deposition of Hafnium and Zirconium Oxides Using Metal Amide Precursors. *Chem. Mater.* **2002**, *14* (10), 4350−4358.
(42) Silvennoinen, R. J.; Jylhä, O. J. T.; Lindblad, M.; Sainio, J. P.; Puurunen, R. L.; Krause, A. O. I. Atomic Layer Deposition of Iridium (III) Acetylacetonate on Alumina, Silica-Alumina, and Silica Supports. *Appl. Surf. Sci.* **2007**, *253* (9), 4103−4111.
(43) Vuori, H.; Lindblad, M.; Krause, A. O. I. Preparation of Noble Metal Catalysts by Atomic Layer Deposition: FTIR Studies. *Stud. Surf. Sci. Catal.* **2006**, *162*, 505−512.
(44) Vuori, H.; Silvennoinen, R. J.; Lindblad, M.; Österholm, H.; Krause, A. O. I. Beta Zeolite-Supported Iridium Catalysts by Gas Phase Deposition. *Catal. Lett.* **2009**, *131* (1), 7−15.
(45) Jeong, N. C.; Lee, J. S.; Tae, E. L.; Lee, Y. J.; Yoon, K. B. Acidity Scale for Metal Oxides and Sanderson's Electronegativities of Lanthanide Elements. *Angew. Chem., Int. Ed.* **2008**, *47* (52), 10128−10132.
(46) Li, Y.; Lan, Y.; Cao, K.; Zhang, J.; Wen, Y.; Shan, B.; Chen, R. Surface Acidity-Induced Inherently Selective Atomic Layer Deposition of Tantalum Oxide on Dielectrics. *Chem. Mater.* **2022**, DOI: 10.1021/acs.chemmater.2c00851.
(47) Armini, S.; Loyo Prado, J.; Krishtab, M.; Conard, T.; Meersschaut, J.; Le, Q. T.; Verdonck, P.; Baklanov, M. R. Study of Wet Surface Activation Routes to Enable the Deposition of Monomolecular Organic Thin Films on k 2.0 Porous Dielectrics. *Ecs J. Solid State Sc.* **2014**, *3* (1), N3106−N3111.
(48) Sun, Y.; Krishtab, M.; Mankelevich, Y.; Zhang, L.; De Feyter, S.; Baklanov, M.; Armini, S. Surface-Confined Activation of Ultra Low-k Dielectrics in CO_2 Plasma. *Appl. Phys. Lett.* **2016**, *108* (26), 262902.
(49) Heo, J.; Lee, S. Y.; Eom, D.; Hwang, C. S.; Kim, H. J. Enhanced Nucleation Behavior of Atomic-Layer-Deposited Ru Film on Low-k Dielectrics Afforded by UV-O_3 Treatment. *Electrochem. Solid. St.* **2008**, *11* (2), G5.
(50) Shoeb, J.; Kushner, M. J. Mechanisms for Sealing of Porous Low-k SiOCH by Combined He and NH_3 Plasma Treatment. *J. Vac. Sci. Technol. A* **2011**, *29* (5), 051305.
(51) Choi, C. K.; Kim, C. Y.; Navamathavan, R.; Lee, H. S.; Woo, J.-K.; Hyun, M. T.; Lee, H. J.; Jeung, W. Y. UV Irradiation Effects on the Bonding Structure and Electrical Properties of Ultra Low-k SiOC(-H) Thin Films for 45 nm Technology Node. *Curr. Appl. Phys.* **2011**, *11* (5), S109−S113.
(52) Heo, J.; Eom, D.; Kim, H. J. UV-O_3 Treatment Effects on Structural Changes of Low-k Thin Films. *Microelectron. Eng.* **2007**, *84* (9), 2188−2191.
(53) Sekiguchi, A.; Kobayashi, A.; Koide, T.; Okada, O.; Hosokawa, N. Reaction of Copper Oxide and β-Diketone for In Situ Cleaning of Metal Copper in a Copper Chemical Vapor Deposition Reactor. *Jpn. J. Appl. Phys.* **2000**, *39* (11R), 6478.
(54) de Paula, C.; Richey, N.; Zeng, L.; Bent, S. F. Mechanistic study of nucleation enhancement in atomic layer deposition by pretreatment with small organometallic molecules. *Chem. Mater.* **2020**, *32* (1), 315−325.